Energy Proceedings
Vol 50, 2025
ISSN 2004-2965

Investigation on Collaborative Optimization Strategy based on PCM-Air Composite Cooling Battery Thermal Management System#

Guangliang Wang[1], Jun Zhao[12*], Jing Wang[1], Lei Gu[1], Juan Song[1], Jintao Niu[1]

1 Key Laboratory of Efficient Utilization of Low and Medium Grade Energy (Tianjin University), Tianjin 300350, China

2 National Industry-Education Platform of Energy Storage, Tianjin University, Tianjin 300350, China

(Corresponding Author: zhaojun@tju.edu.cn)

ABSTRACT

In order to make full use of the latent heat of phase change material (PCM) and reduce loss of active cooling power consumption, based on synergy idea, this study discusses the influence of three air supply strategies of air-cooling start time, air-cooling stop time and air-cooling velocity on the composite cooling effect. Based on the entropy weight method, the optimal air supply strategy in the above three schemes is selected. The results show that after optimizing the air supply strategy, the PCM utilization rate of three schemes is increased by 52.50%, 29.13% and 31.44% respectively. The loss of air-cooling power consumption is reduced by 52.61%, 18.72% and 31.44% respectively. In particular, the strategy of adjusting the inlet velocity of battery module has the best comprehensive target performance, and the OP value is 0.64. The maximum temperature and maximum temperature difference after discharge are 307.55 K and 2.66 K, respectively. In general, it is feasible to optimize the composite cooling scheme based on the idea of synergy.

Keywords: PCM cooling, air cooling, battery thermal management, optimization strategy

NONMENCLATURE

Abbreviations	
BESS	Battery Energy Storage System
BTM	Battery Thermal Management
PCM	Phase Change Material
Symbols	
c_p	specific heat capacity, $J \cdot kg^{-1} \cdot K^{-1}$
f_{PCM}	PCM liquid fraction, %
k	turbulent kinetic energy, $m^2 \cdot s^{-2}$
P_{fan}	fan power consumption, kJ
$q_{V,b}$	battery heat generation, $W \cdot m^{-3}$
T	temperature, K
t	time, s
U	velocity, $m \cdot s^{-1}$
ε	turbulent dissipation rate, $m^2 \cdot s^{-3}$
λ	thermal conductivity, $W \cdot m^{-1} \cdot K^{-1}$
μ	dynamic viscosity, $N \cdot s \cdot m^{-2}$
ρ	density, $kg \cdot m^{-3}$

1. INTRODUCTION

Lithium-ion batteries are widely used in BESSs due to their high energy density, long cycle life and low self-discharge rate. In order to achieve high efficiency, it is necessary to control the temperature of battery between 288.15 K and 308.15 K [1]. Excessive temperature will accelerate battery aging and affect life expectancy. Too low temperature will increase the internal resistance and affect performance. At present, the main measures of battery thermal management (BTM) include air cooling, liquid cooling, PCM cooling and heat pipe cooling. Air cooling [2] has the advantages of simple structure and low cost, but its relatively low cooling efficiency limits its further application. Compared with air cooling, liquid cooling [3] has higher heat transfer efficiency, but it has the problems of complex structure design of cooling pipeline and easy leakage of coolant. Heat pipe [4] cooling mainly relies on high-performance heat conduction process to achieve battery heat dissipation, but the high cost limits its large-scale application.

PCM cooling [5] has attracted more attention due to its advantages of light weight, good temperature control effect and no need to consume additional energy. Khateeb et al. [6] added aluminum metal foam to PCM to enhance the thermal conductivity of PCM. Cheng et al. [7] explored the thermal conductivity of composite PCM with different mass fractions of expanded graphite. Sun et al. [8] proposed a new type of fin structure based on the characteristics of straight fins and arc fins. Compared

This is a paper for the 16th International Conference on Applied Energy (ICAE2024), Sep. 1-5, 2024, Niigata, Japan.

with the single PCM thermal management system, the novel fins could extend the working time by 54%-90% during the discharge process. However, when the battery is discharged at a higher rate, the heat generation exceeds the upper limit of PCM storage heat, resulting in PCM cooling failure. At this time, the problem can be solved by using PCM cooling combined with air cooling or liquid cooling. Ahmad et al. [9] proposed a cylindrical metal fin for enhanced composite cooling heat dissipation. The effects of PCM thickness, number and diameter of fins on BTM were studied. Chen et al. [10] compared thermal characteristics of battery under four schemes: no PCM cooling, single PCM cooling, single air cooling and composite cooling. The results showed that the core temperature of battery under composite cooling scheme is reduced by 15.9 K.

Most of the existing research on composite cooling aims to improve the overall heat dissipation performance of cooling system. There are few studies on the synergistic optimization strategy of mutual cooperation between active and passive cooling. Wang et al. [11] studied PCM-liquid composite cooling. When the liquid cooling inlet flow rate is 0.0016 kg/s, the melting rate of PCM is only 8% during the discharge process. Zheng et al. [12] found that the heat absorption of PCM accounted for less than 10% in the composite cooling of PCM and liquid, and the heat absorption of liquid cooling accounted for up to 80%.

The above studies show that overall heat dissipation performance of composite cooling system can generally meet the requirements of BTM at higher rates. However, the proportion of heat absorbed between the active and passive cooling schemes is not balanced. The proportion of active cooling heat dissipation is far greater than that of passive cooling. PCM is often not fully and effectively utilized. Therefore, in order to make full use of the latent heat advantage of PCM and reduce the power loss of the fan, this study discuss the influence of three air supply schemes of air-cooling start time, air-cooling stop time and air-cooling velocity on the composite cooling effect based on the synergy idea.

2. NUMERICAL SIMULATIONS

2.1 *Physical model*

Fig. 1 shows the BTM physical model of PCM-air composite cooling. The battery parameters are from the literature of Xin et al. [13]. The size of battery pack is 148 × 81 × 92 mm. A battery module is composed of 24 battery packs in series. The size of battery module is 544 × 374 × 234 mm. The distance between each battery pack and between the battery pack and side walls of battery module is 10 mm. The PCM is arranged in the longitudinal side area of each battery pack. The PCM is positioned numbered 1-6 along the air-cooled flow direction. In addition, the thickness of PCM is 6 mm. The melting temperature and latent heat of PCM are 303.15 K-305.15 K and 150 kJ/kg. The physical parameters of the remaining materials are shown in Table 1.

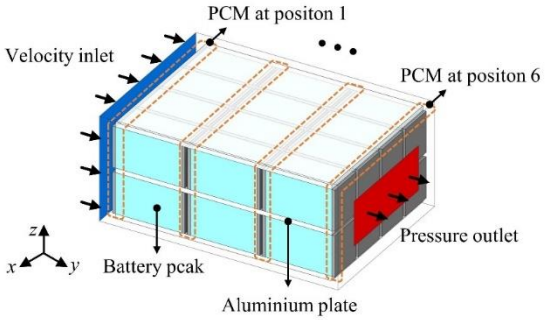

Fig. 1 BTM model of PCM-air composite cooling

Table 1 Physical parameters of materials in battery module.

Materials	ρ	c_p	λ	μ
Air	1.225	1006.43	0.0242	1.79×10^{-5}
Battery	2300	1072	1.5, 18.5, 18.5	/
Aluminum plate	2719	871	202.4	/
PCM	1000	2000	1.2	/

2.2 *Mathematical model*

2.2.1 Battery heat generation model

The energy equation of battery calculation zones is expressed as follows.

$$\frac{\partial}{\partial t}\left(\rho_{\mathrm{b}} c_{p,\mathrm{b}} T\right)=\nabla\cdot\left(\lambda_{\mathrm{b}}\nabla T\right)+q_{V,\mathrm{b}} \tag{1}$$

As shown in Eq. 1, there is a source term q_V in the energy equation of batteries. Xin et al. [13] tested the heat generation rate of battery by calibration calorimetry method based on heat transfer theory and energy conservation law, as shown in Eq. 2.

$$\begin{aligned} q_{V,\mathrm{b}} &= 26408.12838-32.29395t+0.02572t^2 \\ &\quad -8.77507\times10^{-6}t^3+1.15957\times10^{-9}t^4 \end{aligned} \tag{2}$$

2.2.2 PCM model

The equivalent heat capacity method is used to analyze PCM model. The heat transfer differential equation in PCM zones is as follows.

$$\rho_{\mathrm{PCM}} c_{p,\mathrm{PCM}}\frac{\partial T}{\partial t}=\nabla\cdot\left(\lambda_{\mathrm{PCM}}\nabla T_{\mathrm{PCM}}\right)+\rho_{\mathrm{PCM}} L_{\mathrm{PCM}}\frac{\partial f_{\mathrm{PCM}}}{\partial t} \tag{3}$$

The f_{PCM} in Eq. 3 can be calculated by Eq. 4.

$$f_{\mathrm{PCM}}=\begin{cases} 0 & T\le T_{\mathrm{s}} \\ \dfrac{T-T_{\mathrm{s}}}{T_{\mathrm{l}}-T_{\mathrm{s}}} & T_{\mathrm{s}}\le T\le T_{\mathrm{l}} \\ 1 & T\ge T_{\mathrm{l}} \end{cases} \tag{4}$$

2.2.3 Air cooling model

The mass, momentum and energy equations in the air calculation zones are shown in Eq. 5-7, respectively.

$$\frac{\partial \rho}{\partial t}+\rho\nabla\cdot\vec{U}=0 \tag{5}$$

$$\frac{\partial}{\partial t}\left(\rho\vec{U}\right)+\rho\nabla\cdot\left(\vec{U}\vec{U}\right)=-\nabla p+\mu\nabla\cdot\left(\nabla\vec{U}\right)+\rho\vec{g} \tag{6}$$

$$\rho c_p\left(\frac{\partial T}{\partial t}+\vec{U}\cdot\nabla T\right)=\nabla\cdot\left(\lambda\nabla T\right) \tag{7}$$

In this study, the inlet Reynolds number of battery module is 30789. Therefore, the standard *k-ε* model is chosen to describe the turbulence flow of air. The calculation methods of turbulent kinetic energy *k* and dissipation rate *ε* are shown in Eq. 8 and Eq. 9.

$$\frac{\partial}{\partial t}(\rho k)+\frac{\partial}{\partial x_j}(\rho k\mu_j)=\frac{\partial}{\partial x_j}\left(\left(\mu+\frac{\mu_t}{\sigma_k}\right)\frac{\partial k}{\partial x_j}\right)+G_k+G_b-\rho\varepsilon-Y_M \tag{8}$$

$$\frac{\partial}{\partial t}(\rho\varepsilon)+\frac{\partial}{\partial x_j}(\rho\varepsilon\mu_j)=\frac{\partial}{\partial x_j}\left(\left(\mu+\frac{\mu_t}{\sigma_\varepsilon}\right)\frac{\partial \varepsilon}{\partial x_j}\right)+C_{1\varepsilon}\frac{\varepsilon}{k}(G_k+C_{3\varepsilon}+G_b)-\rho C_{2\varepsilon}\frac{\varepsilon^2}{k} \tag{9}$$

2.3 *Initial and boundary conditions*

In this study, the ambient temperature is set to 298.15 K. The initial temperature of the battery, PCM and air is consistent with the ambient temperature. The velocity inlet and pressure outlet are set as the boundary conditions. The air velocity and temperature of inlet is 1.57 m/s and 298.15 K, respectively.

2.4 *Model validation*

2.4.1. Grid independence

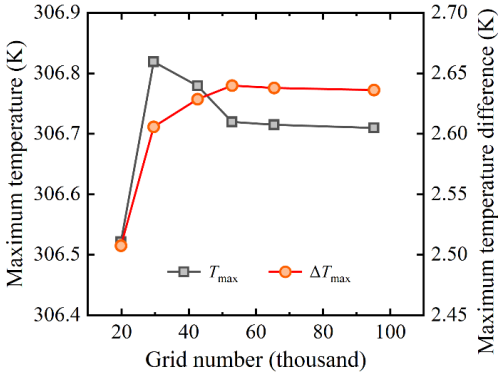

Fig. 2 Grid independence

Fig. 2 shows the comparison results of the maximum temperature and maximum temperature difference of battery module under different grid numbers. When the number of grids is greater than 52864, the error of the maximum temperature and maximum temperature difference caused by continuing to increase the number of grids is less than 0.01 K. Therefore, in order to save the calculation time, this study finally divides calculation model into 52864 grids.

2.4.2. Battery heat generation model

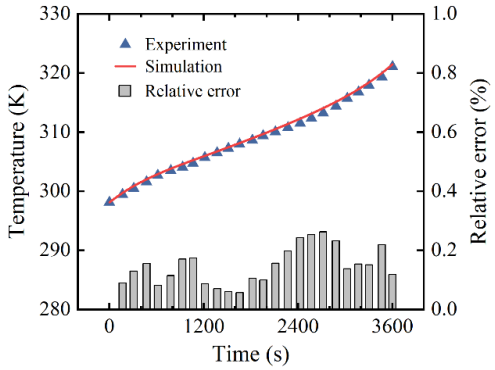

Fig. 3. Comparison of simulation and experiment

In order to verify the accuracy of the numerical results, this study chooses the experiment of Xin et al. [13] for comparison. The results of comparison between this study and experiment are shown in Fig. 3. It can be seen that the numerical results are consistent with the experimental results. The absolute difference of average temperature of battery does not exceed 1 K, and the relative error does not exceed 0.5%. Therefore, the results show that the present mathematic model is feasible to analyze the thermal performance of batteries.

3. RESULTS AND DISCUSSION

3.1 Composite cooling analysis

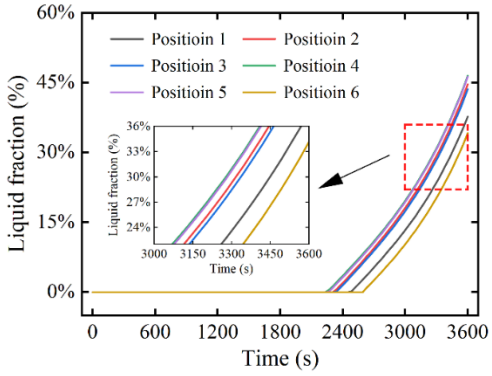

Fig. 4. PCM liquid fraction

At the end of the discharge, the maximum temperatures of single air cooling and composite cooling are 308.68 K and 306.72 K, respectively. When the single air cooling is used, the maximum temperature of system exceeds the upper limit of BTM temperature of 0.53 K. After the composite cooling scheme is adopted, the maximum temperature is reduced by 1.96 K. In terms of temperature uniformity, the maximum temperature differences of single air cooling and composite cooling are 2.81 K and 2.64 K, respectively. Compared with the single air cooling, the temperature uniformity of composite cooling scheme is increased by 6.05%.

Furthermore, the liquid fraction of PCM in the composite cooling scheme is discussed, as shown in Fig. 4. At the end of discharge, the liquid fraction of PCM at six positions is 37.74%, 44.68%, 43.63%, 46.54%, 46.30% and 34.18%, respectively. The liquid fraction of all PCM does not exceed 50%, which indicates that the existing composite cooling scheme does not give full play to the passive cooling capacity of PCM. In order to make full use of the latent heat advantage of PCM and reduce the power loss of the fan, this study further discusses the influence of three air supply strategies, air-cooling start time, air-cooling stop time and air-cooling velocity, on the composite cooling effect.

3.2 Delay air-cooling start time

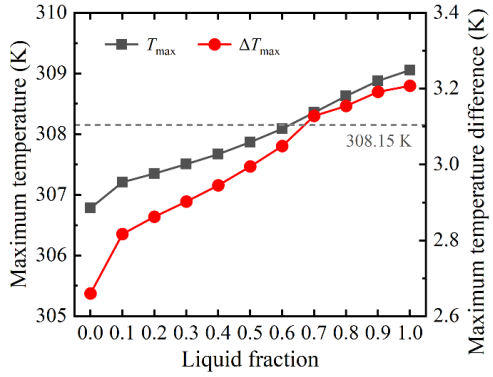

Fig. 5. Temperature characteristics of start time

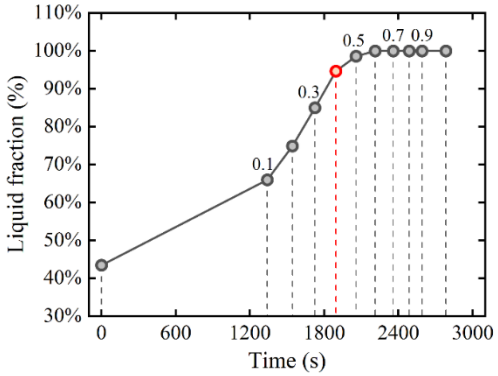

Fig. 6. PCM liquid fraction of start time

In order to select the best start time of air-cooling system, Fig. 5 and Fig. 6 show the temperature characteristics of battery and the liquid fraction of PCM, respectively. It can be seen that when PCM liquid fraction is larger, the air-cooling system is started, and the maximum temperature and maximum temperature difference are worse. However, the PCM utilization rate of system is higher at this time. When considering the requirements of the BTM temperature range, the maximum temperature exceeds upper limit temperature when the liquid fraction of PCM exceeds 0.6. From the perspective of PCM utilization, when the liquid fraction of PCM is 0.1, 0.2 and 0.3, the air cooling is started. After the discharge, the liquid fraction of PCM in the system is 66.01%, 74.93% and 85.01%, respectively. The latent heat of some PCM is still not fully utilized.

Therefore, considering the two factors, the final choice is to start the air-cooling heat dissipation system when the PCM liquid fraction is 0.4. At this time, the maximum temperature and maximum temperature difference of battery module are 307.67 K and 2.94 K, respectively. The utilization rate of PCM is 94.68%. Besides, the air-cooling start time corresponding to the PCM liquid fraction of 0.4 is 1894 s. Compared with the air supply strategy before optimization, the power consumption of fan is reduced by 52.61%.

3.3 Early air-cooling stop time

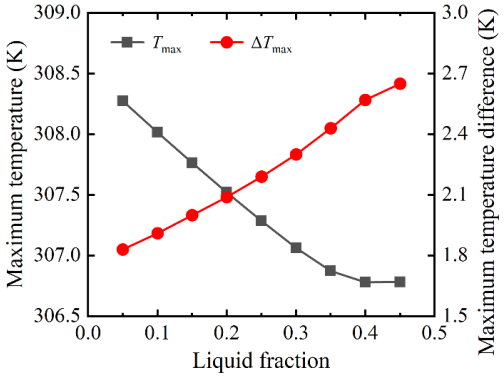

Fig. 7. Temperature characteristics of stop time

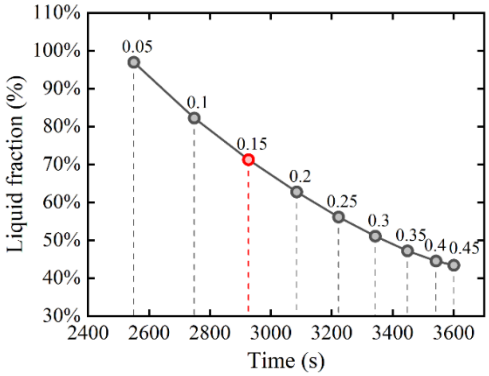

Fig. 8. PCM liquid fraction of stop time

It can be seen from Fig. 7 and Fig. 8 that when the PCM liquid fraction is larger, the air-cooling system is stopped, and the maximum temperature is also lower. However, the maximum temperature difference shows an upward trend with the increase of PCM liquid fraction. This is mainly because PCM cooling has better system temperature uniformity than air cooling. In addition, the delay of stop time causes a significant increase in fan power consumption and a significant decrease in PCM utilization.

Finally, when considering requirements of BTM temperature range, when the PCM liquid fraction is 0.05 and 0.10, stopping the air-cooling system causes to have

a higher maximum temperature value of 308.28 K and 308.02 K. From the perspective of PCM utilization, when the PCM liquid fraction is 0.20, 0.25, 0.30, 0.35, 0.40 and 0.45, the air-cooling system is stopped. After the discharge, the PCM liquid fraction is 62.82%, 56.17%, 51.11%, 47.27%, 44.61% and 43.47%, respectively. At this time, the utilization rate of PCM is significantly insufficient. Considering the two factors, the final choice is to stop the air-cooling heat dissipation system when the PCM liquid fraction is 0.15. At this time, the maximum temperature and maximum temperature difference of battery module after discharge are 307.77 K and 2.00 K, respectively. The utilization rate of PCM is 71.31%. Besides, the air-cooling stop time corresponding to the PCM liquid fraction of 0.15 is 2926 s. The power consumption of fan is reduced by 18.72% compared with that before optimization of air supply strategy.

3.4 Change air-cooling velocity

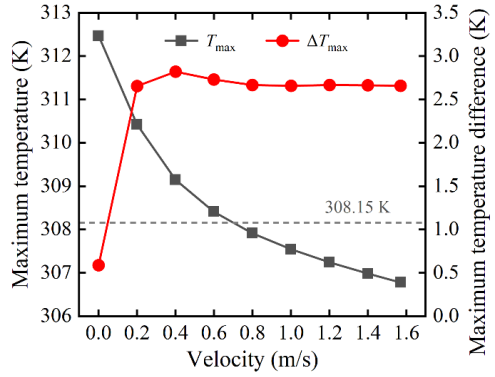

Fig. 9. Temperature characteristics of changing velocity

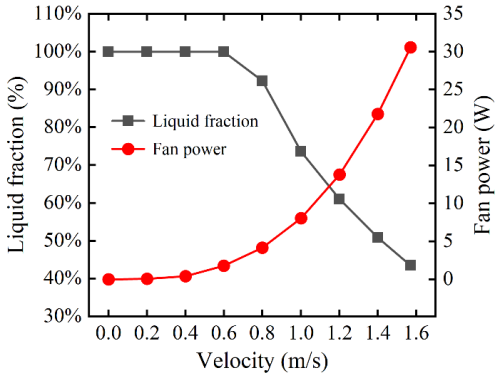

Fig. 10. PCM liquid fraction of changing velocity

Fig. 9 and Fig. 10 show temperature characteristics of battery module and power loss of fan at the end of discharge, respectively. It can be seen that the greater inlet velocity, the lower the maximum temperature. However, the decrease of maximum temperature is decreasing, and there is a marginal effect. When the velocity increases from 0 m/s to 0.2 m/s, the maximum temperature decreases by 2.05 K. When the velocity increases from 1.4 m/s to 1.57 m/s, the maximum temperature only decreases by 0.20 K. Combined with Fig. 11, the fast velocity can cause a significant increase in the power consumption of fan.

Finally, from the perspective of BTM temperature range, when the velocity is less than 0.8 m/s, the battery has a larger maximum temperature after discharge. From the perspective of fan power consumption and PCM utilization, when the velocity is 1.2m/s, 1.4m/s and 1.57m/s, the utilization of PCM after discharge is 61.04%, 50.86% and 43.47%, respectively. At this time, the utilization of PCM is significantly insufficient, and the power consumption loss of fan is greater. Considering the above three aspects, the velocity of battery module is finally determined to be 1.0 m/s. At this time, the maximum temperature and maximum temperature difference are 307.55 K and 2.66 K, respectively. The utilization rate of PCM is 73.62%. Besides, the power consumption of fan is reduced by 69.97% compared with that before optimization of air supply strategy.

3.5 Optimization strategy selection

Through the above analysis and discussion, Table 2 summarizes the effects of three air supply strategies on battery temperature characteristics, PCM utilization rate and fan power consumption. From the perspective of BTM temperature uniformity, the system temperature uniformity using air-cooling stop time strategy is the best. The maximum temperature difference is only 2.00 K. But the fan power consumption is 87.64 kJ. From the perspective of fan power loss, when the velocity of battery module inlet is 1.0 m/s, the fan power consumption of system is 33.06 kJ. However, the temperature uniformity is relatively poor at this time. The maximum temperature difference is 2.66 K.

Further, in order to select the air supply strategy with better comprehensive performance, this study calculates the weights corresponding to maximum temperature, the minimum temperature, the maximum temperature difference, liquid fraction and fan power consumption based on entropy weight method. Finally, the optimal scheme can be selected by analyzing the score of the comprehensive target performance OP. The calculation method is shown in Eq. 10.

$$OP = 0.23T_{max} + 0.20T_{min} + 0.25\Delta T_{max} + 0.16f_{PCM} + 0.16P_{fan} \quad (10)$$

According to the Eq. 10, the OP scores of the above three air supply strategies are calculated to be 0.21, 0.61 and 0.64, respectively. The calculation results show that changing inlet velocity of battery module has better comprehensive target performance when considering the temperature performance of BTM, improving the

utilization rate of PCM and reducing the power consumption of fan.

Table 2 Optimization strategy summary.

Type	T_{max}	T_{min}	ΔT_{max}	f_{PCM}	P_{fan}
Start time	307.68	304.73	2.95	94.68	51.10
Stop time	307.78	305.78	2.00	71.31	87.64
Velocity	307.55	304.89	2.66	73.62	33.06

4. CONCLUSION

In order to make full use of the latent heat advantage of PCM in composite cooling and reduce the loss of air-cooling power consumption, based on the idea of synergy, this study deeply discusses the influence of three air supply strategies on the composite cooling effect. The main conclusions are as follows.

(1) PCM-air composite cooling system has better temperature performance than single air-cooling system. After adopting the composite cooling scheme, the maximum temperature and the maximum temperature difference of battery module are reduced by 1.96 K and 0.17 K, respectively. The temperature uniformity is increased by 6.05%.

(2) Compared with before optimization of air supply strategy, when air-cooling start-up time is 1894 s, the utilization rate of PCM is increased by 52.50%. The power consumption is reduced by 52.61%. When air-cooling stop time is 2926 s, the utilization rate of PCM is increased by 29.13%. The power consumption is reduced by 18.72%. When velocity at the inlet of battery module is 1.0 m/s, the utilization rate of PCM is increased by 31.44%. The power consumption is reduced by 69.97%.

(3) From perspective of meeting BTM temperature performance, improving PCM utilization and reducing fan power consumption, the strategy of changing inlet velocity of battery module has better comprehensive target performance, and the OP value is 0.64.

ACKNOWLEDGEMENT

This work was supported by the National Natural Science Foundation of China (No. 52206271) and the National Natural Science Foundation of China (No.52306266).

REFERENCE

[1] Chen D, Jiang J, Kim G-H, Yang C, Pesaran A. Comparison of different cooling methods for lithium ion battery cells, Applied Thermal Engineering, 94 (2016) 846-854.

[2] Chen K, Zhang Z, Wu B, Song M, Wu X. An air-cooled system with a control strategy for efficient battery thermal management, Applied Thermal Engineering, 236 (2024) 121578.

[3] Yin B, Zuo S, Xu Y, Chen S. Performance of liquid cooling battery thermal management system in vibration environment, Journal of Energy Storage, 53 (2022) 105232.

[4] Weragoda DM, Tian G, Burkitbayev A, Lo K-H, Zhang T. A comprehensive review on heat pipe based battery thermal management systems, Applied Thermal Engineering, 224 (2023) 120070.

[5] Lin X-W, Zhou Z-F, Liu T-F, Xue S-Q, Liang Y, Zhang L-F, Liu B. Rate capability and Ragone plots for designing battery thermal management system based on phase change material, Journal of Energy Storage, 74 (2023) 109539.

[6] Khateeb SA, Amiruddin S, Farid M, Selman JR, Al-Hallaj S. Thermal management of Li-ion battery with phase change material for electric scooters: experimental validation, Journal of Power Sources, 142 (2005) 345-353.

[7] Cheng W-l, Zhang R-m, Xie K, Liu N, Wang J. Heat conduction enhanced shape-stabilized paraffin/HDPE composite PCMs by graphite addition: Preparation and thermal properties, Solar Energy Materials and Solar Cells, 94 (2010) 1636-1642.

[8] Sun Z, Fan R, Zheng N. Thermal management of a simulated battery with the compound use of phase change material and fins: Experimental and numerical investigations, International Journal of Thermal Sciences, 165 (2021) 106945.

[9] Ahmad S, Liu Y, Khan SA, Hao M, Huang X. Hybrid battery thermal management by coupling fin intensified phase change material with air cooling, Journal of Energy Storage, 64 (2023) 107167.

[10] Chen S, Wang R, Bao H, Roskilly AP, Ma Z. Numerical investigation of form-stable composite phase change material for battery passive cooling, Case Studies in Thermal Engineering, 50 (2023) 103410.

[11] Wang Y, Gao T, Zhou L, Gong J, Li J. A parametric study of a hybrid battery thermal management system that couples PCM with wavy microchannel cold plate, Applied Thermal Engineering, 219 (2023) 119625.

[12] Zheng Y, Shi Y, Huang Y. Optimisation with adiabatic interlayers for liquid-dominated cooling system on fast charging battery packs, Applied Thermal Engineering, 147 (2019) 636-646.

[13] Xin Q, Yang T, Zhang H, Yang J, Zeng J, Xiao J. Experimental and numerical study of lithium-ion battery thermal management system using composite phase change material and liquid cooling, Journal of Energy Storage, 71 (2023) 108003.